DNA-Origami Enabled Distance-Dependent Sensing

Jeanne E. van Dongen*, Jan C.T. Eijkel and Loes I. Segerink

BIOS Lab on a Chip Group, MESA+ & TechMed Institutes, Max Planck Center for Complex Fluid Dynamics, University of Twente, 7500 AE Enschede, The Netherlands

*j.e.vandongen@utwente.nl

https://orcid.org/0000-0001-9350-0394

***Abstract*—Localized surface plasmon resonance is a popular optical detection technique due to its ease of use. However, the main issues of this technique are its selectivity and sensitivity towards (small) single molecules. We address these challenges by introducing a distance-dependent plasmonic sensing method based on a gold nanoparticle (AuNP) tethered by a single DNA hairpin to a gold film (Au-film). The plasmonic properties of a AuNP enable us to distinguish the z-height of the particle. In the absence of a target sequence, the hairpin keeps the AuNP close to the Au-film, while hybridization with a target sequence results in an extended state of the DNA tether. We experimentally confirmed the assembly of this sensor and by simulations, predicted the plasmonic signal of the two states. Finally, we showed experimental results as proof of concept of our sensing method.**

Keywords—single molecule sensing, plasmonics, AuNPs, hairpin origami

I. Introduction

Optical single molecule sensors are gaining ground in several medical applications due to their promise of sensitivity and accuracy [1], [2]. Especially label-free sensing techniques based on surface plasmon resonance (SPR) have been studied extensively, including localized surface plasmon resonance (LSPR) [3]. Methods based on (L)SPR measure the binding of an analyte as a change in the (local) refractive index, which results in a shift of the corresponding extinction or scattering.

The high sensitivity towards small changes in refractive index is both an advantage and a disadvantage of these sensor types. Both specific and non-specific adsorption changes the local refractive index, making it impossible to distinguish between these two by simple readout [4]. Furthermore, for single biomarker monitoring, (L)SPR lacks sensitivity towards small molecules, like DNA. With available labeling methods, both the sensitivity and selectivity issues can be tackled; however, these labeling methods generally experience coupling-distance limitations and/or comprise multiple assay steps [5].

To address these challenges, we present a single-step biomolecule sensing method (**Figure 1**). Previously, we have theoretically shown by simulations that this measurement principle, which is based on changes in the distance between a gold nanoparticle (AuNP) and a gold film (Au-film), can be used to target the binding of a single biomarker molecule [6]. The Au-film acts as a mirror when the same AuNP is placed near a Au-film. This allows the AuNP to interact with its mirror image, resulting in a red shift, comparable to the spectral shift observed for AuNP dimers [7], [8]. The degree of red shift of the AuNP scattering spectrum is strongly distance-dependent, which makes this system extremely suitable to probe changes in z-height of the AuNP [9], [10],

This work is sponsored by The Weijerhorst foundation, The Netherlands

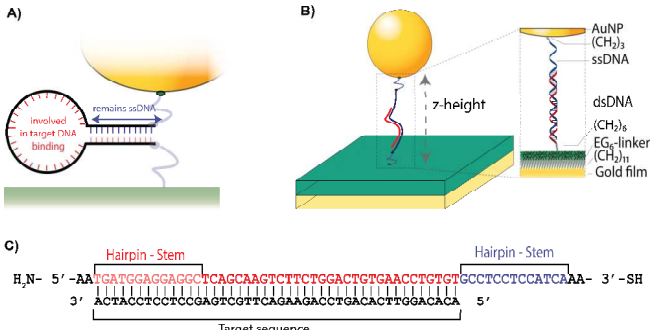

Fig 1: **Schematic representation of single-step single stranded DNA (ssDNA) sensing with AuNP-DNA conjugates** A) ssDNA molecule bound to the Au-film and AuNP. Upon target binding, part of the self-complementary DNA nucleotides will bind to the target (in red), unzipping the hairpin and resulting in a ssDNA (in blue) tether followed by a double stranded DNA (dsDNA) tether. B) Detailed schematic overview of a single sensing element bound to a target DNA sequence. C) Hairpin DNA sequence, with corresponding 5' end (-NH_2 modified), and the 3' end (-SH) modifications.

In the presented sensing method, we exploit AuNPs tethered to a Au-film by a ssDNA hairpin. The hairpin will keep the AuNP close to the Au-film, without much rotational freedom. When a target sequence hybridizes and unzips the hairpin, this results in an extension of the contour length of the DNA tether but also in more rotational freedom. The tether consists of several linkers parts, including a part of 13 nts ssDNA that adds enormous flexibility to the tether and allows different configurations that all contribute to the average z-height of a Au-film tethered AuNP. Other than our previous work, where we proposed a dynamic readout needing an advanced laser-equipped setup, the readout in this work is enabled by a simple color camera.

II. Experimental

A. Chemicals

11-Mercapto-tetra(ethyleneglycol)undecanol (HS-C_{11}-$(EG)_5$-OH) and 11-mercapto-hexa(ethylene glycol) undecyloxy acetic acid (HS-C_{11}-$(EG)_6$-OCH_2-COOH) were purchased from Prochimia (Gdansk, Poland). N-hydroxysuccinimide (NHS) and 1-ethyl-3-(3-dimethylaminopropyl)carbodiimide hydrochloride (EDC) were purchased from Fisher Scientific (Landsmeer, the Netherlands). Phosphate buffered saline (PBS, Bioperformance Certified pH 7.4), 2-mercaptoethanol, and absolute ethanol were purchased from Sigma Aldrich

2022 IEEE Sensors | 978-1-6654-8464-0/22/$31.00 ©2022 IEEE | DOI: 10.1109/SENSORS52175.2022.9967092

(Zwijndrecht, the Netherlands). Gold nanoparticles (AuNPs, 80 nm in diameter, optical density=1) were purchased from BBIsolutions (Crumlin, United Kingdom).

B. Sensor preparation

SPR chips (Ssense) were piranha (H_2SO_4:H_2O_2 3:1) cleaned for ~ 30 seconds, quenched in deionized (DI) water, then rinsed with a copious amount of DI water and absolute ethanol before blow drying in an N_2 stream. The cleaned and dried substrates were placed in a UV-ozone oven for 20 minutes, after which the chips were immediately soaked into a total of 2mM ethanol solution of carboxyl- and hydroxyl-terminated oligo(ethylene glycol) (OEG) thiols overnight. After overnight incubation and self-assembled monolayer (SAM) formation, the SPR chip was rinsed with copious amounts of ethanol and DI water and dried in a stream of N_2.

C. Darkfield microscopy

Darkfield microscopy imaging was performed on an inverted Olympus GX71 microscope using reflection mode, using a 20× darkfield objective, darkfield filter cube and with a 2× magnifier lens. Pictures were acquired using a Zeiss Axiocam HRc (Jena,Germany) spatial scanned color camera.

III. Results and Discussion

Successful assembly of the sensor was confirmed by Quartz Crystal Microbalance (QCM) monitoring, as can be seen in **Figure 2**. Prior to QCM measurements, a Au-coated QCM sensor was functionalized with mixed OEG SAMs, where the $HS(CH_2)_{11}(C_2H_5O)_6COOH$ thiol served as a functional site to react with the amine groups of the hairpin and $HS(CH_2)_{11}(C_2H_5O)_5OH$ thiol served to prevent non-specific interaction of, for example, the target sequence.

Carboxyl groups do not directly react with amines, and therefore the mounted QCM sensors underwent an EDC/NHS activation step (step I) of the SAMs prior to hairpin immobilization (step II). After hairpin immobilization, the 80 nm AuNPs were added (step III), which can form a thiol-Au bond with the 3' end of the DNA-hairpin. To passivate the AuNP surface, mercapto-ethanol was flushed over (step IV), however, full passivation cannot be confirmed using this technique, and could also result in

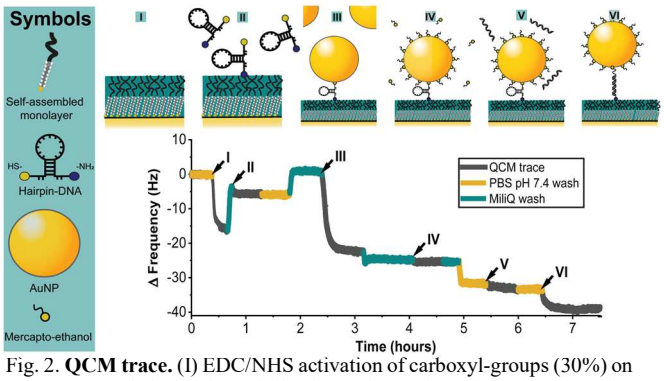

Fig. 2. **QCM trace.** (I) EDC/NHS activation of carboxyl-groups (30%) on SAMs, (II) hairpin immobilization via activated carboxyl–amine coupling, (III) AuNP immobilization via AuNP-thiol coupling, (IV) passivation of AuNPs with β-mercapto-ethanol, (V) no binding of non-complementary DNA, (VI) binding of complementary DNA.

displacement of the ssDNA-thiol-AuNP bond that keeps the AuNP tethered to the Au-film. Finally, the specificity of the sensor was confirmed by flushing over 1 µM of non-target sequence (step V, ~0.2 Hz difference) and 1 µM target sequence (step VI, ~10 Hz difference).

To numerically predict the performance of our assay, we estimated the z-height distribution of a AuNP tethered to the Au-film via DNA either in the hairpin- or the "extended"-state using a Monte Carlo simulation method [6]. Distinguishing between the hairpin state and the "extended" state is crucial for the success of this assay. The hairpin state will keep the AuNP close to the Au-film, without much rotational freedom. When a target sequence hybridizes and unzips the hairpin, this results in an extension of the contour length of the DNA tether, but also in more rotational freedom. Another important issue is, that in a color camera detection assay, sensitivity mainly depends on the position of the resonance peak in relation to the spectral response of the camera, and its RGB filters [11], and not only on the z-height of the AuNP. Therefore we multiplied the spectral sensitivity for the red and green channel of the camera with the distance-dependent plasmonic response of a AuNP above a Au-film, predicted by electromagnetic Boundary Element Method (BEM) simulations [11]. Combining the AuNP height-dependent red/green ratio with the z-height distribution, results in a prediction of the red/green ratio shift we could expect for the hairpin and extended-state DNA, corresponding to no-target bound and target sequence bound respectively (**Figure 3B**). Unfortunately, the color camera is not able to probe the largest spectral changes while varying the AuNP z-height, which are found around 770 nm in the infrared part of the spectrum (**Figure 3A**).

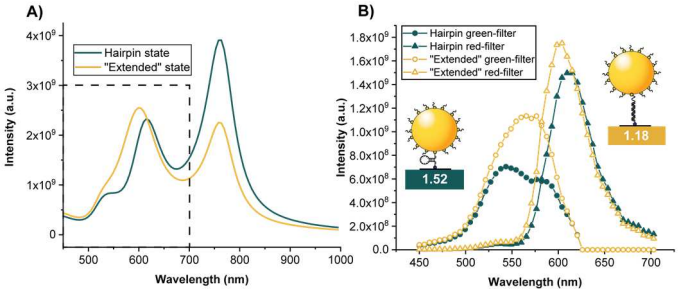

Fig. 3. **Predicted red/green response of the hairpin and "extended" state.** 10,000 states were generated with the Monte-Carlo simulations, each resulting in a z-height of the AuNP above the Au-film (see Figure 3). The z-height probability distribution that results from these simulations is used to predict, by electromagnetic BEM simulation, A) the average AuNP spectrum. Here the dashed box indicates the part of the spectra covered by the color camera. B) AuNP scattering spectra corrected for the spectral sensitivity of the AXIOCAM HR color camera.

Next, we experimentally investigated the capability of our sensor to follow target binding to the hairpin, measured as a change in the color camera-measured red/green ratio of the AuNP scattering. We assembled the sensor on an SPR gold coated substrate, and for imaging and incubation with the target sequence in buffer, we applied a CoverWell™ press-on incubation chamber on the substrate. Since we used an inverted microscope, and since darkfield imaging is a very light-inefficient technique, we decided not to image through the semi-transparent Au-film of the SPR chip but flip the chip with an incubation chamber.

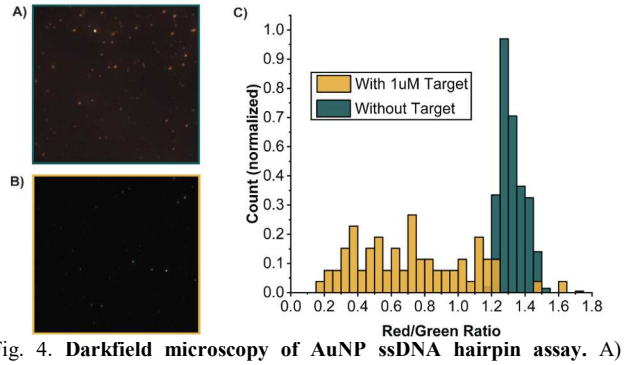

Fig. 4. **Darkfield microscopy of AuNP ssDNA hairpin assay.** A) Darkfield image before the addition of the 1 µM target solution. B) Darkfield image after 1.5 hours of incubation with 1 µM ssDNA target. C) Normalized count of the red/green ratio of the individual AuNPs as depicted in A and B. Without the target, a red/green ratio of 1.30 ± 0.08 was observed, and after the addition of the target, a shift in the red/green ratio to 0.82 ± 0.31 was observed.

We started with imaging of the hairpins without a target sequence in buffer (**Figure 4a**), after which we removed the chip from the microscope and added the same buffer, supplemented with 1 µM ssDNA target to the incubation chamber. After 1 hour of incubation time, we took darkfield pictures of the AuNPs (**Figure 4b**). With an in-house developed MATLAB script, we determined the red/green ratio of the individual particles before and after incubation with the target sequence (**Figure 4c**).

We performed two experiments, and in both experiments, we found a red/green ratio prior to target binding that was very similar to the red/green ratio predicted by the simulations, although it was slightly lower (**Figure 3** (1.51) vs. **Figure 4** (1.30 ± 0.08) and (1.38 ± 0.16) (data not shown).

As the Monte Carlo simulations combined with the electromagnetic BEM simulations predicted, we observed an overall decrease in the red/green ratio after the ssDNA target introduction. Besides this shift in the red/green ratio, we also observed the disappearance of the typical "doughnut" shape scattering pattern, originating from the polarization to the single AuNP light scattering [12] This strongly supports a displacement of the AuNP from the Au-film induced by target sequence binding. However, the distribution of red/green ratios observed upon target binding was much broader than that of red/green ratio distribution in the hairpin state. The red/green ratio shift was also much more extensive than expected from simulations. The origin of these much broader variations in the red/green ratio and more significant shift for the "extended" state could not be fully explained (yet). The following section discusses several system properties that could cause these observations.

Firstly, our Monte Carlo model includes no particle-movement-related information and might be oversimplified. Due to the short tether length used in this study, it could be that substrate-particle interactions like hydrodynamic effects [13], [14], any effects related to the DLVO theory [15], [16], volume exclusion effects [17] and/or unknown effects that cannot be explained yet [18] cause the AuNPs to behave differently than expected from simulations.

Secondly, the scattering spectra obtained from the electromagnetic BEM simulations also result from a rough approximation of the experimental settings [19]. Several factors influence the scattering properties of an individual AuNP above a Au-film, which could differ from the simulated conditions, like the AuNP size, the light source's angle of incidence [20] and the effect of the Au-film roughness [21].

Thirdly, our assay procedure could influence the observed deviations, as the chip was removed from the microscope and realigned after buffer replacement. This could result in slight changes in the focusing height, also influencing the angle of incidence of the incoming light. Furthermore, the AuNPs seem to scatter much less light after adding the target sequence, making (re)focusing harder upon hairpin-target complementation.

IV. Conclusionsions and Outlook

Here, we have shown proof of the principle of using DNA-origami for distance-dependent biomolecule detection. For ssDNA sensing, both the hairpin opening and the successful chemical assembly of the sensor were confirmed. Furthermore, a preliminary experiment with darkfield microscopy indicated a clear difference in red/green ratio upon target addition. The difference in red/green ratio upon target addition is more prominent than expected by the simulations due to (yet) unknown causes.

As a current readout method, we used a color camera that has a spectral sensitivity between 450-700 nm. However, the most considerable spectral changes while varying the AuNP z-height are found around 770 nm in the infrared part of the spectrum. In the future, using filters and/or spectroscopy techniques would make it possible to probe the peak around 770 nm or the ratio between the peak at 770 nm vs. 580 nm to determine the AuNP z-height. Furthermore, recording single particle scattering spectra can help optimize the electromagnetic BEM and Monte Carlo simulations, facilitating a better understanding of the system's behavior and the large variations we currently observe.

Besides the readout method, also the incubation protocol can be improved. In current experiments, we used an incubation chamber, imaged the sensor with buffer only, removed it from the microscope, replaced the buffer with one containing a 1 µM target sequence, and imaged it again. For future experiments, it would be beneficial to have a continuous flow cell that allows one to track the red/green ratio of single AuNPs at one spot over time. In addition, a flow cell with continuous measuring would also rule out issues regarding focusing differences between chips.

Lastly, if resolving between both states appears to be an issue, we could optically follow the dynamics of tethered AuNPs by decreasing the camera's acquisition time. As already discussed, unzipping the hairpin induced by target sequence hybridization adds enormous flexibility to the DNA tether, which can be probed dynamically [6].

Acknowledgments

We want to thank Robert Molenaar for assistance during darkfield imaging, Cees Otto and Jorien Berendsen for fruitful discussions, and Laurens Spoelstra for assistance with the Monte Carlo simulations.

REFERENCES

[1] N. Akkilic, S. Geschwindner, and F. Höök, "Single-molecule biosensors: Recent advances and applications," *Biosensors and Bioelectronics*, vol. 151. 2020, doi: 10.1016/j.bios.2019.111944.

[2] G. Luka *et al.*, "Microfluidics integrated biosensors: A leading technology towards lab-on-A-chip and sensing applications," *Sensors (Switzerland)*, vol. 15, no. 12. MDPI AG, pp. 30011–30031, Dec. 01, 2015, doi: 10.3390/s151229783.

[3] A. B. Taylor and P. Zijlstra, "Single-Molecule Plasmon Sensing: Current Status and Future Prospects," *ACS Sensors*, vol. 2, no. 8. pp. 1103–1122, 2017, doi: 10.1021/acssensors.7b00382.

[4] K. A. Willets and R. P. Van Duyne, "Localized surface plasmon resonance spectroscopy and sensing," *Annu. Rev. Phys. Chem.*, vol. 58, pp. 267–297, Apr. 2007, doi: 10.1146/annurev.physchem.58.032806.104607.

[5] E. Petryayeva and U. J. Krull, "Localized surface plasmon resonance: Nanostructures, bioassays and biosensing-A review," *Analytica Chimica Acta*, vol. 706, no. 1. pp. 8–24, 2011, doi: 10.1016/j.aca.2011.08.020.

[6] J. E. van Dongen, L. R. Spoelstra, J. T. W. Berendsen, J. T. Loessberg-Zahl, J. C. T. Eijkel, and L. I. Segerink, "A Multiplexable Plasmonic Hairpin-DNA Sensor Based on Target-specific Tether Dynamics," *ACS Sensors*, vol. 6, no. 12, pp. 4297–4303, Dec. 2021, doi: 10.1021/acssensors.1c02097.

[7] R. E. Armstrong, J. C. Van Liempt, and P. Zijlstra, "Effect of Film Thickness on the Far- A nd Near-Field Optical Response of Nanoparticle-on-Film Systems," *J. Phys. Chem. C*, vol. 123, no. 42, pp. 25801–25808, 2019, doi: 10.1021/acs.jpcc.9b06592.

[8] J. J. Mock, R. T. Hill, Y.-J. Tsai, A. Chilkoti, and D. R. Smith, "Probing Dynamically Tunable Localized Surface Plasmon Resonances of Film-Coupled Nanoparticles by Evanescent Wave Excitation," *Nano Lett*, vol. 12, p. 14, 2012, doi: 10.1021/nl204596h.

[9] E. W. A. Visser, M. Horáček, and P. Zijlstra, "Plasmon Rulers as a Probe for Real-Time Microsecond Conformational Dynamics of Single Molecules," *Nano Lett.*, vol. 18, no. 12, pp. 7927–7934, 2018, doi: 10.1021/acs.nanolett.8b03860.

[10] J. J. Mock, R. T. Hill, A. Degiron, S. Zauscher, A. Chilkoti, and D. R. Smith, "Distance-dependent plasmon resonant coupling between a gold nanoparticle and gold film," *Nano Lett.*, vol. 8, no. 8, pp. 2245–2252, 2008, doi: 10.1021/nl080872f.

[11] K. L. Göeken, V. Subramaniam, and R. Gill, "Enhancing spectral shifts of plasmon-coupled noble metal nanoparticles for sensing applications," *Phys. Chem. Chem. Phys.*, vol. 17, no. 1, pp. 422–427, Dec. 2015, doi: 10.1039/c4cp03739a.

[12] J. J. Mock, R. T. Hill, A. Degiron, S. Zauscher, A. Chilkoti, and D. R. Smith, "Distance-dependent plasmon resonant coupling between a gold nanoparticle and gold film," *Nano Lett.*, vol. 8, no. 8, pp. 2245–2252, 2008, doi: 10.1021/nl080872f.

[13] S. Kumar, C. Manzo, C. Zurla, S. Ucuncuoglu, L. Finzi, and D. Dunlap, "Enhanced Tethered-Particle Motion Analysis Reveals Viscous Effects," *Biophys. J.*, vol. 106, no. 2, pp. 399–409, Jan. 2014, doi: 10.1016/j.bpj.2013.11.4501.

[14] M. Manghi, C. Tardin, J. Baglio, P. Rousseau, L. Salomé, and N. Destainville, "Probing DNA conformational changes with high temporal resolution by tethered particle motion," *Phys. Biol.*, vol. 7, no. 4, p. 046003, Oct. 2010, doi: 10.1088/1478-3975/7/4/046003.

[15] E. J. W. Verwey, "Theory of the stability of lyophobic colloids," *J. Phys. Colloid Chem.*, vol. 51, no. 3, pp. 631–636, 1947, doi: 10.1021/j150453a001.

[16] B. Derjaguin and L. Landau, "Theory of the stability of strongly charged lyophobic sols and of the adhesion of strongly charged particles in solutions of electrolytes," *Prog. Surf. Sci.*, vol. 43, no. 1–4, pp. 30–59, May 1993, doi: 10.1016/0079-6816(93)90013-L.

[17] D. E. Segall, P. C. Nelson, and R. Phillips, "Volume-exclusion effects in tethered-particle experiments: Bead size matters," *Phys. Rev. Lett.*, vol. 96, no. 8, p. 088306, Mar. 2006, doi: 10.1103/PhysRevLett.96.088306.

[18] S. Brinkers, "All that glitters is gold," 2011.

[19] J. Waxenegger, A. Trügler, and U. Hohenester, "Plasmonics simulations with the MNPBEM toolbox: Consideration of substrates and layer structures," *Comput. Phys. Commun.*, vol. 193, pp. 138–150, 2015, doi: 10.1016/j.cpc.2015.03.023.

[20] D. Y. Lei *et al.*, "Revealing plasmonic Gap modes in particle-on-film systems using dark-field spectroscopy," *ACS Nano*, vol. 6, no. 2, pp. 1380–1386, 2012, doi: 10.1021/nn204190e.

[21] C. Lumdee, B. Yun, and P. G. Kik, "Effect of surface roughness on substrate-tuned gold nanoparticle gap plasmon resonances," *Nanoscale*, vol. 7, no. 9, pp. 4250–4255, Feb. 2015, doi: 10.1039/c4nr05893c.